ChemPhysChem

Research Article
doi.org/10.1002/cphc.202200429

Chemistry Europe
European Chemical Societies Publishing

www.chemphyschem.org

First-principles study of the magnetic exchange forces between the RuO_2(110) surface and Fe tip

Qiuhua Liang,[a, c] Geert Brocks,*[b, c, d] and Anja Bieberle-Hütter*[a, b]

Magnetic exchange force microscopy (MExFM) is an important experimental technique for mapping the magnetic structure of surfaces with atomic resolution relying on the spin-dependent short-range exchange interaction between a magnetic tip and a magnetic surface. RuO_2 is a significant compound with applications in heterogeneous catalysis and electrocatalysis. It has been characterized recently as an antiferromagnetic (AFM) material, and its magnetism has been predicted somewhat surprisingly to play an important role in its catalytic properties. In the current study, we explore theoretically whether MExFM can visualize the magnetic surface structure of RuO_2. We use density functional theory (DFT) calculations to extract the exchange interactions between a ferromagnetic Fe tip interacting with an AFM RuO_2(110) surface, as a function of tip-surface distance and the position of the tip over the surface. Mimicking the MExFM experiment, these data are then used to calculate the normalized frequency shift of an oscillating cantilever tip versus the minimum tip-surface distance, and construct corrugation height line profiles. It is found that the exchange interaction between tip and surface is strongest for a parallel configuration of the spins of the tip and of the surface; it is weakest for an anti-parallel orientation. In a corrugation profile, this gives rise to a sizable height difference of 25 pm between the spin-up and spin-down Ru atoms in the RuO_2(110) surface at a normalized frequency shift $\gamma = -10.12\,\mathrm{fNm}^{1/2}$. The O atoms in the surface are not or hardly visible in the corrugation profile.

Introduction

Ruthenium dioxide (RuO_2) is a metal that has been successfully applied in various fields, such as electrocatalysis,[1] heterogeneous catalysis,[2] Li-ion batteries,[3] and supercapacitors.[4] Its favorable properties encompass its capability for reversible redox reactions, a high proton conductivity, a large specific capacitance, and a high thermal and chemical stability.[5] In many of these application, reactions and processes that take place at the surface of RuO_2 play a decisive role.[6] RuO_2 has a rutile structure and most of our current understanding of the processes and reactions at RuO_2 surfaces is based on the (110) surface, since that is the crystal surface with minimum surface energy.[5,7] Bulk RuO_2 and the RuO_2(110) surface have long been assumed to be non-magnetic.[8] Recently, bulk single-crystal RuO_2 has been found to be anti-ferromagnetic (AFM) at room temperature.[9,10] DFT studies show that the antiferromagnetism persists at the (110) surface and that the spin states of the surface Ru atoms affect the catalytic activity of the surface, such as the oxygen evolution reaction of water splitting.[11,12] So far, the antiferromagnetism of the RuO_2(110) surface has not been demonstrated experimentally.

Magnetic exchange force microscopy (MExFM) is an extension of non-contact atomic force microscopy, which aims at probing the spin-dependent short-range interaction between a probe tip and a surface. MExFM has allowed to map out the magnetic properties of nanostructures at surfaces with atomic-scale resolution.[13–16] MExFM is essentially an AFM equipped with a magnetic tip; the strength of the short-range exchange interaction between tip and surface depends on whether the spins on the atoms of the surface are parallel to those in the tip or anti-parallel. Keeping the magnetization of the tip constant, the direction and strength of the magnetic moments on the surface atoms can then be mapped out by scanning the surface with the tip.

MExFM is usually applied in tapping mode, with the tip attatched to a cantilever oscillating near its resonance frequency near the surface of the sample. Using a feedback loop the minimal cantilever-surface distance is controlled by keeping the frequency of the oscillating cantilever constant, which then gives a topological magnetic image of the surface. In experi-

[a] Dr. Q. Liang, Dr. A. Bieberle-Hütter
Electrochemical Materials and Interfaces (EMI), Dutch Institute for Fundamental Energy Research (DIFFER), De Zaale 20, 5612 AJ, Eindhoven, the Netherlands
E-mail: a.bieberle@differ.nl
[b] Prof. Dr. G. Brocks, Dr. A. Bieberle-Hütter
Center for Computational Energy Research (CCER), P.O. Box 513, 5600 MB, Eindhoven, the Netherlands
E-mail: g.h.l.a.brocks@utwente.nl
[c] Dr. Q. Liang, Prof. Dr. G. Brocks
Materials Simulation and Modeling (MSM), Department of Applied Physics, Eindhoven University Technology, P.O. Box 513, 5600MB, Eindhoven, the Netherlands
[d] Prof. Dr. G. Brocks
Computational Materials Science, Faculty of Science and Technology and MESA + Institute for Nanotechnology, University of Twente, P.O. Box 217, 7500 AE Enschede, the Netherlands

Supporting information for this article is available on the WWW under https://doi.org/10.1002/cphc.202200429

ments, MExFM has been successfully used to resolve the atomic scale AFM structure of the NiO(001) surface[13,17] and the magnetic structure of a Fe monolayer on the W(001) surface, for instance.[14,15]

The corrugation amplitude of the topological image depends on the properties of the cantilever. In order to compare experimental results with different cantilevers and/or different oscillation amplitudes and frequencies, or to link theoretical calculations with experiments, a normalized frequency shift γ is introduced, see the methods section for more details. For the case of a Fe tip and a NiO(001) surface, Kaiser et al.[13] have reported a corrugation amplitude of 4.5 pm at a normalized frequency shift $\gamma = -2.55\,\mathrm{fNm}^{1/2}$, and Pielmeier and Giessibl[17] have reported a corrugation amplitude of 1.1 pm at $\gamma = -0.25\,\mathrm{fNm}^{1/2}$, demonstrating the sensitivity of MExFM.

Based upon a microscopic model of the surface and using a Fe cluster to mimic the ferromagnetic Fe tip, DFT calculations have been used to obtain the spin-dependent exchange force between tip and surface, and, based upon this, the normalized frequency shift and the topological magnetic image of the surface. This has been done for the Fe tip and NiO(001) surface system,[18–20] and for the Fe tip and Fe monolayer on W(001) surface system, for instance.[14,21] For the former system, Granovskij et al.[18,20] have reported a corrugation amplitude of 25 pm at $\gamma = -22.0\,\mathrm{fNm}^{1/2}$.

In this work, we use spin-polarized DFT to study the exchange interaction between a FM Fe tip and an AFM RuO_2(110) surface. The exchange energy and force are calculated as function of tip-surface distance for several positions of the tip over the surface. Based upon these data, the normalized frequency shifts γ are calculated as a function of minimal tip-surface approach distance, which are then used to calculate the corrugation height profiles for different values of a fixed γ, as one would do in a MExFM experiment. We compare our results with the results obtained for the NiO(001) surface. Our results offer guidelines for the experimental detection and understanding of magnetism of the RuO_2(110) surface.

Computational Details

All calculations are performed with DFT using projector augmented waves (PAW) as implemented in the Vienna Ab initio Software Package (VASP).[22–24] As PAW potentials, we use the Ru_pv and Fe_pv potentials for Ru and Fe atoms, which include p semi-core states, and the standard PAW potential for the O atom. All plane waves up to a kinetic energy cutoff of 500 eV are included in the basis set. The spin-polarized generalized gradient approximation (GGA) functional of Perdew-Burke- Ernzerhof (PBE) is used to describe exchange and correlation.[25] We perform GGA+U calculations, with U terms based on the scheme of Dudarev et al.[26] On-site Coulomb/exchange energy parameters of $U - J = 2.0$ eV[9] and 4.3 eV[27] are used for the Ru and Fe atoms, respectively.

The DFT optimized lattice constants of bulk RuO_2 are $a = 4.51$ Å, $c = 3.12$ Å, which are in good agreement with the experimental values of $a = 4.49$ Å, $c = 3.11$ Å.[28] Cutting the bulk RuO_2 along the [110] direction, a five-layer stoichiometric slab with RuO_2(110) surfaces is constructed, see Figure 1(a), which has a surface unit cell with lattice parameters $a = 3.12$ Å, $b = 6.41$ Å. The top surface of this slab, which has a maximum exposure of Ru atoms, is then used to probe the surface. Note that we do not use the surface structure covered by oxygen bridges, as is used in several DFT studies of RuO_2 in the literature (see, e.g., Ref. [11]), Partially O- or OH-covered RuO_2 surfaces are stable under wet conditions. However, the oxygen atoms do not acquire a magnetic moment.[12] Such adsorbed oxygen species then shield the Ru atoms, which do have a sizeable magnetic moment. As MExFM relies on short-range spin-dependent interactions, adsorption of oxygen species will obstruct measuring the surface magnetism. This also implies that – if MExFM measurements will be carried out in the future – the RuO_2 surface needs to be maximally cleaned of adsorbed oxygen, including the oxygen bridges found on the (110) surface.

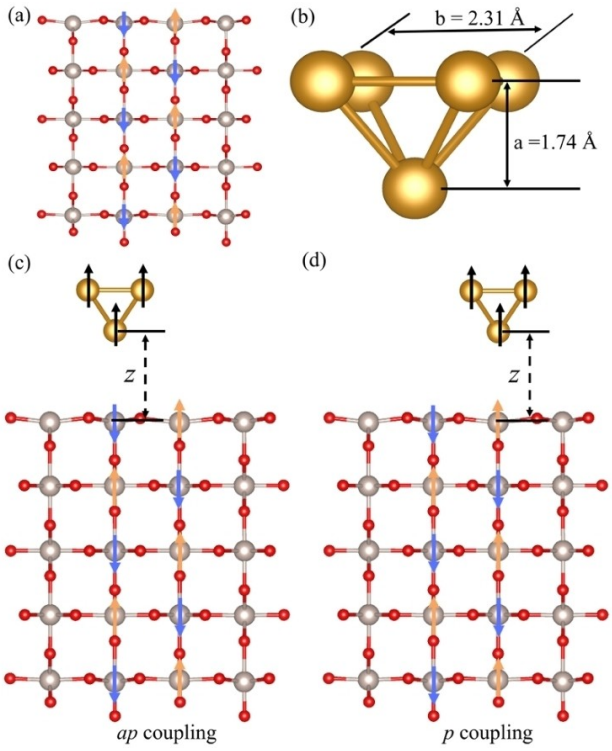

Figure 1. (a) Side view of the RuO_2 slab with (110) surfaces at the top and bottom. The anti-ferromagnetic ordering of magnetic moments on the Ru atoms is indicated by orange and blue arrows. (b) Optimized structure of the Fe tip. Side views of the (c) antiparallel (*ap*) coupling and (d) parallel (*p*) coupling of the RuO_2(110) surface and the Fe tip; z is the distance between the centers of the tip apex atom and the surface Ru atom underneath. Red: O, grey: Ru, brown: Fe.

The optimized lattice constant of bulk bcc Fe is 2.83 Å, in good agreement with the experimental value of 2.87 Å.[29] The Fe tip is modeled by a Fe cluster in bcc (001) orientation containing five Fe atoms, as shown in Figure 1(b). Before coupling the RuO_2(110) surface and the Fe tip, we optimize the surface and tip separately. After optimization, we obtain a tip structure with $a = 1.74$ Å and $b = 2.31$ Å, see Figure 1(b), which is consistent with previous results.[30] The magnetic moment of the apex Fe atom is 3.36 μ_B, and that of the other four Fe atoms is 3.30 μ_B, all significantly larger than the magnetic moment of 2.22 μ_B in bulk bcc Fe.[31] The total magnetic moment of the five-atom tip is 16.56 μ_B.

This tip is then brought into proximity of the surface, see Figures 1(c), and (d). A vacuum region of at least 15 Å is added above the surface to allow the tip to move away from the surface without interacting with the latter's periodic image. Likewise, lateral

interactions between periodic images are suppressed by using an in-plane 3×2 surface supercell, with dimensions 9.36×12.83 Å. While varying the tip-surface distance, we do not relax the surface and tip geometries. A $4\times3\times1$ Monkhorst-Pack sampling of the reciprocal space is used. Convergence tests regarding the size of the slab and the supercell can be found in our previous work.[12] The magnetic ordering and the magnetic moments on the Ru atoms in the slab are presented in the Supporting Information Figure S1 and Table S1. Anti-parallel and parallel coupling between the magnetic moments on the tip and specific Ru atoms of the RuO_2(110) surface are illustrated in Figures 1(c) and (d).

In order to understand the chemical and magnetic interaction between the Fe tip and the (110) surface, we calculate the magnetic exchange energy $E_{ex}(z)$ and force $F_{ex}(z)$. The exchange energy is obtained from the DFT total energies of the antiparallel (*ap*) and parallel (*p*) configurations between tip and surface by calculating the difference between the two total energy curves[21,33]

$$E_{ex}(z) = E_{ap}(z) - E_{p}(z), \tag{1}$$

where z is the distance between the centers of the tip apex atom and a surface Ru atom underneath without structural relaxations, see Figure 1. Positive and negative signs for $E_{ex}(z)$ correspond to preferential *p* and *ap* coupling, respectively. Similarly, the exchange force F_{ex} is defined as[21,33]

$$F_{ex}(z) = F_{ap}(z) - F_{p}(z), \tag{2}$$

with $F_{ap}(z)$ and $F_{p}(z)$ the total forces on the tip along the z direction of the *ap* and *p* systems, respectively. Positive values of $F_{ex}(z)$ indicate a more attractive interaction for the *p* coupling than for the *ap* coupling.

Calculating the exchange forces and energy only makes sense, if the tip cluster carries a stable magnetic moment. The total magnetic moment of the Fe tip cluster after coupling with the RuO_2(110) surface, the magnetic moment of the apex Fe atom are shown in Figure S2. For tip-surface distances $z > 3.2$ Å, the apex atom has a magnetic moment of 3.32–3.38 and the tip cluster has a total magnetic moment of ~16.56 μ_B, values very close to those of a free-standing Fe tip cluster. For shorter distances, the surface and tip atoms start to hybridize appreciably, which decreases the magnetic moments on the tip, although for $2.2 < z < 3.2$ Å, they are still within 10% of their free-standing values. The magnetic moments of the surface Ru atoms also change for shorter distances because of the tip-surface interaction. The magnetic moment on the Ru↑atom decreases considerably with decreasing distance, see Figure S3. The magnetic moment on the Ru↓atom also decreases with decreasing distance, but to a lesser degree, Figure S3, before it increases again for $z < 2.7$ Å. This already indicates that the tip-surface interaction for the *p* coupling is stronger than for the *ap* one.

The topographic map of the surface can be obtained when scanning the surface while maintaining a constant frequency shift of the MExFM cantilever. To be able to compare results obtained with different cantilevers, a normalized frequency shift is defined that does not depend strongly on the elementary properties of the cantilever (eigenfrequency, spring constant, oscillation amplitude). In the large amplitude limit the normalized frequency shift can be expressed as[20,34–36]

$$\gamma(d) = \frac{1}{\sqrt{2}\pi} \int_{d}^{\infty} \frac{F_{ts}(z)}{\sqrt{z-d}} dz, \tag{3}$$

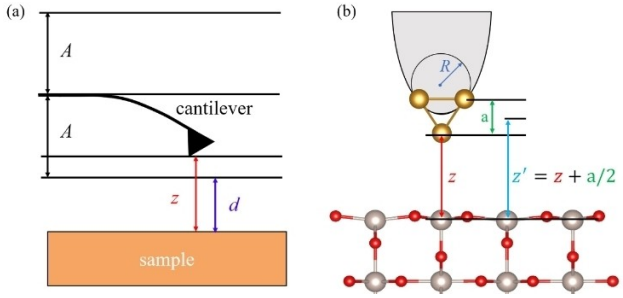

Figure 2. (a) Schematic drawing of an oscillating cantilever with a tip; *A* is the oscillation amplitude, *z* is the distance between the tip and the surface, and *d* is the minimum tip-surface distance during the oscillation. (b) Microscopic model of an Fe tip over a RuO_2(110) surface; *a* is the vertical height of the Fe tip cluster. Long-range van der Waals (vdW) forces are modeled using a continuum parabolic tip where z' is the distance between tip and surface, and *R* is its curvature radius.

where d is the minimum tip-surface distance during one oscillation cycle. A schematic drawing of the cantilever with tip, and the distances z and d is shown in Figure 2(a). $F_{ts}(z)$ is the total force between tip and surface, which is the sum of a short-range chemical term, $F_{sr}(z)$, and a long-range Van der Waals (vdw) term, $F_{vdw}(z)$,[20]

$$F_{ts}(z) = F_{sr}(z) + F_{vdw}(z). \tag{4}$$

As short-range term $F_{sr}(z)$, we use the forces on the Fe cluster tip, $F_{ap}(z)$ or $F_{p}(z)$, as obtained from the DFT calculations.

To calculate the vdw forces one can use a simplified model, consisting of a macroscopic parabolic tip and a planar surface[14,20]

$$F_{vdw}(z) = -\frac{A_H R}{6\left(z+\frac{a}{2}\right)^2}, \tag{5}$$

where R is the radius of curvature of the tip (we use $R = 10$ nm), and a is a height correction that results from the Fe cluster sticking out from the tip, see Figure 2(b); A_H is the Hamaker constant, for which we use the value 1.865×10^{-19}, following Ref. [20]

A corrugation height profile can be obtained by (numerically) inverting $\gamma(d)$ to $d(\gamma)$, and repeating the calculations for every position x, y of the tip over the surface, giving a function $d(\gamma, x, y)$, where the function at fixed γ then represents a corrugation height profile. Because of the heavy computational demands, we perform these calculations only for a restricted number of x, y positions, namely those that correspond to positions of surface atoms. Defining the magnetization of the tip as spin-up (↑), we use the Ru atom with its magnetic moment spin-down (↓) as reference. Using the minimum tip-surface distance above the Ru↓ atom $d(\gamma, \text{Ru}\downarrow)$ as the reference point, we then define

$$\Delta d(\gamma, \text{X}) = d(\gamma, \text{X}) - d(\gamma, \text{Ru}\downarrow), \tag{6}$$

where X marks the position of a surface atom, Ru↑ or O.

Results and Discussions

The DFT total energies and forces on the tip cluster are shown in Figures 3(a) and (b) for tip-surface distances in the range

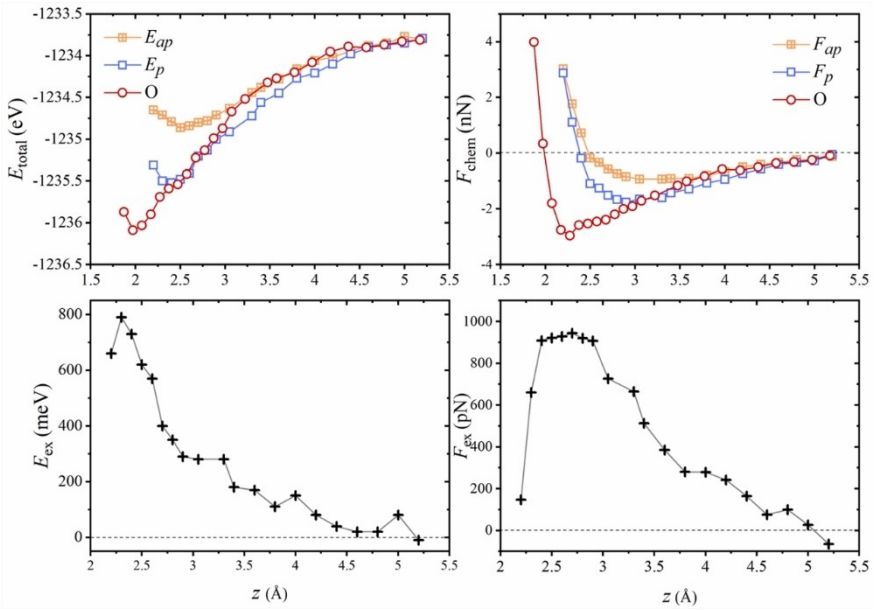

Figure 3. The (a) total energy of the Fe tip - RuO_2(110) system and (b) total force on the tip, above the Ru atoms *ap* and *p* configurations, and above an O site, as a function of the tip-surface distance; (c) the exchange energy $E_{ex}(z)$ and (d) exchange force $F_{ex}(z)$ vs *z*.

$2.2 \leq z \leq 5.2$ Å and three different positions *x*, *y* of the tip over the surface. The subscripts *ap* and *p* represent the positions over a Ru↓ and a Ru↑ atom, respectively; O stands for the position over a surface O atom. At distances $z > 4.4$ Å, the difference in total energy between these positions is small, see Figure 3(a), and generally increases with decreasing *z*. Above the Ru↓ and Ru↑ sites, the total energies reach a minimum at $z = 2.5$ Å and 2.4 Å, respectively, and then increase again, showing the hallmark of a typical chemical binding energy curve. The total energy of the tip above the O site also decreases as the tip approaches the surface and reaches a minimum at $z = 2.0$ Å.

The total force on the tip above the Ru↓ and Ru↑ sites decreases with *z* decreasing from 5.2 Å to 3.0 Å, where it reaches a minimum of −0.93 nN and −1.76 nN, respectively, and then increases again with *z* decreasing from 3.0 Å to 2.2 Å, as shown in Figure 3(b). The total force on the tip above the Ru ↓ and Ru↑ sites is negative for $z > 2.5$ Å, indicating an attractive tip-surface interaction. Likewise, above the O site, the total force decreases first with decreasing tip-surface distance and then increases, reaching a minimum of −2.96 nN at $z = 2.3$ Å. The force is negative for $z > 2.0$ Å, signaling an attractive interaction. The absolute values of these forces are consistent with what is calculated for other systems.[20,30] In the range $2.2 < z < 4.4$ Å, the force for the tip above the Ru↑ atom is more attractive than that of Fe tip above the Ru↓ atom, see Figure 3(b), indicating that the *p* interaction is stronger than the *ap* interaction. The force for the tip above the O atom is more attractive than above the Ru atoms in the range $2.2 < z < 2.9$ Å, while it is less attractive than above the Ru↑ atom in the range $3.2 < z < 4.4$ Å, signaling that the Fe–O interaction is more attractive than the Fe–Ru interaction, but it has a shorter range.

We can compare our results with a similar calculation on an Fe tip - NiO(001) surface, which has a well-known AFM ordering of magnetic moments on the Ni atoms.[13] For NiO(001) at tip-surface distances $2.0 < z < 2.7$ Å, the forces are attractive, their absolute value increases with decreasing distance, is larger for *p* coupling between the tip and a substrate Ni atom, and is largest for a tip position above an O atom.[20] We find the same pattern for the RuO_2(110) surface for tip-surface distances in the range $2.2 < z < 2.9$ Å. For NiO(001) at tip-surface distances $z >$ 2.7 Å, the forces for *ap* coupling become more attractive than for *p* coupling. For the RuO_2(110), we find no such switch; at large distances, the forces for *p* and for *ap* coupling simply converge to the same value.

The exchange energies $E_{ex}(z)$ and $F_{ex}(z)$, calculated from the difference between tip positions above the Ru↓ and Ru↑ atoms, see Eqs. (1) and (2), are plotted in Figures 3(c) and (d). According to Figures 3(c) and (d), the $E_{ex}(z)$ and $F_{ex}(z)$ curves have a similar trend and the exchange interaction between the Fe tip and the Ru atoms increases with decreasing *z*. The exchange energy $E_{ex}(z)$ reaches a maximum of 790 meV at $z =$ 2.3 Å, and then drops again with further decreasing *z*. The exchange force $F_{ex}(z)$ reaches a maximum of 944 pN at $z =$ 2.7 Å, and then also drops with further decreasing *z*. For tip-surface distances $2.4 < z < 2.9$ Å, the exchange force shows a relatively small variation in the range $908 < F_{ex}(z) < 943$ pN, and drops to much smaller values for distances outside this range. The maximum size of the exchange force is quite comparable to the ~1100 pN found between a Fe tip and a NiO(001) surface.[20] In the latter case, this maximum is located in the range 2.0–2.2 Å,[20] reflecting smaller size of the Ni atom as compared to the Ru atom. Based on the positive values for both $E_{ex}(z)$ and $F_{ex}(z)$ (in combination with Eqs. (1) and (2)), it can be concluded that *p* coupling is energetically more

favorable than *ap* coupling for the Fe tip-RuO_2(110) system at all distances $z < 5.0$ Å.

The differences in total energy and forces $E_{ex}(z)$ and $F_{ex}(z)$ between the two surface Ru atoms displayed in Figure 3 may not only be associated with their oppositely oriented magnetic moments. The Ru↓ and Ru↑ atoms at the surface are fivefold, respectively fourfold coordinated by oxygen atoms, see Figure 1 (and Figure S6 for a clearer picture of the structure), so they are structurally slightly different. To distinguish between the pure exchange and the structural effects, we reverse the magnetization of the Fe tip, but keep the magnetic moments in the RuO_2 slab the same, and recalculate $E_{ex}(z)$ and $F_{ex}(z)$. If the two Ru atoms were structurally identical, then upon reversal of the tip magnetization, $E_{ex}(z)$ and $F_{ex}(z)$ should change sign, but not magnitude. Choosing the tip-surface distance $z = 3.6$ Å as an example, E_{ex} changes from $+0.16$ eV to -0.19 eV, and F_{ex} changes from -418 pN to 354 pN. The changes in magnitude are 15–20%, which notably is of the same order as the difference in magnitude between the magnetic moments of the two surface Ru atoms, see Figure S1 and Table S1. We conclude that $E_{ex}(z)$ and $F_{ex}(z)$ partially reflect the structural difference between the two Ru atoms, but that the difference between *p* and *ap* exchange coupling is dominant. Despite their different coordination, and opposite magnetic moments, the two surface Ru atoms have a quite similar electronic structure, see Figure S6. In the following we report on the results obtained with magnetization of the tip up, as in Figure 1.

Is is noticed in Figure 3 that $E_{ex}(z) > 0$, and $F_{ex}(z) > 0$ for $2\text{ Å} < z < 5$ Å, implying that *p* coupling is stronger than *ap* coupling. We suggest the main cause for this is that the minority-spin electrons of the Fe tip couple stronger to the substrate than the majority-spin electrons, see Figure S4, which makes sense as the frontier orbitals of the Fe tip have minority-spin character, see Figure S5. Choosing the magnetization of the tip up, these states then have spin-down character. They can then involve in a Heitler-London (valence bond) interaction with the spin-up states of the surface Ru atoms, which is then stronger for the Ru↑ and for the Ru↓ atoms. The interaction results in a decrease of the magnetic moments on the Ru atoms, as corroborated by Figure S3.

Based on the total force of Figure 3(b), the normalized frequency shift $\gamma(d)$ is calculated according to Eq. (3) for different positions of the Fe tip over the surface; the results are plotted in Figure 4(a). The shapes of the two curves for positions above the Ru↓ and a Ru↑ are similar. Decreasing the minimal tip-surface distance *d* from 5.0 to 2.5 Å decreases the frequency. Note that this region corresponds to the region af attractive tip-surface forces, see Figure 3(b). Decreasing the distance further from 2.5 to 2.2 Å then brings the tip into the region of repulsive tip-surface forces, which increases the frequency again. The absolute value of the frequency shift of the tip position above the Ru↑ site is larger than that of the position above the Ru↑ site, which reflects the stronger tip-surface interaction of the former.

The values for the frequency shift γ obtained for the tip above the O site are more negative than those obtained for the tip above the Ru sites in the range of distances

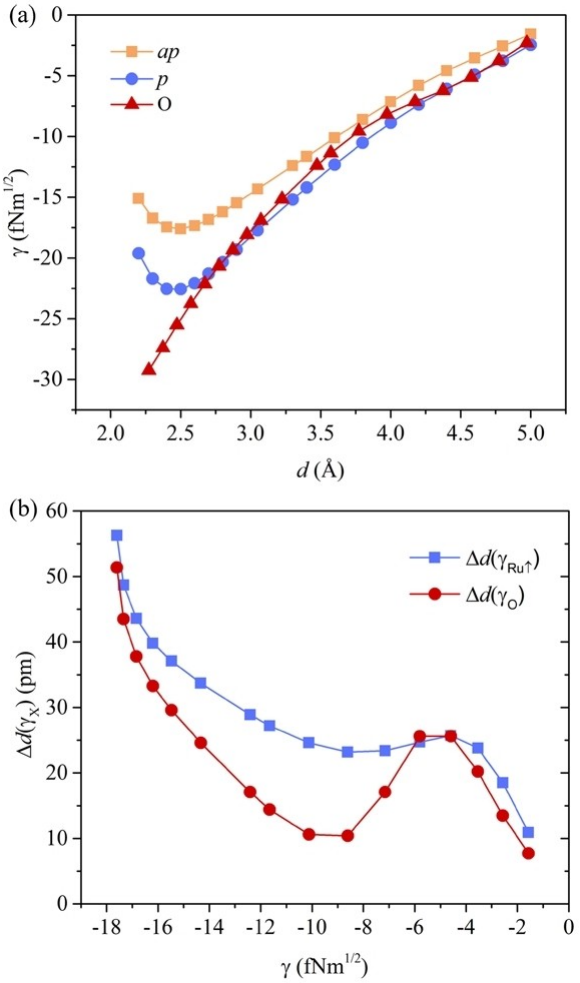

Figure 4. (a) Normalized frequency shift γ as a function of the minimal tip-surface distance *d* for tip positions above the Ru↓, Ru↑ and surface O atoms; (b) tip heights $\Delta d(\gamma, \text{Ru}\uparrow)$ and $\Delta d(\gamma, \text{O})$, calculated by Eq. (6), for tip positions above the Ru↑ and surface O sites, using the Ru↓ site as reference point.

2.2 Å $< d <$ 2.9 Å, Figure 4(a). In the range of 3.0 Å $< d <$ 4.2 Å, the O curve is between the Ru↓ and Ru↑ curves, and in the range of 4.4 Å $< d <$ 5.0 Å it coincides with Ru↓ curve at the range of 4.4 Å $< d <$ 5.0 Å, showing the same trend as the total forces, Figure 4(b).

To mimic an MExFM experiment and extract a corrugation height profile, we have to invert $\gamma(d)$ to $\Delta d(\gamma)$, see Eq. (6). In view of Figure 4(a), this can be done for distances $d \geq 2.5$ Å. We take the Ru↓ curve as reference and calculate the height differences $\Delta d(\gamma, \text{Ru}\uparrow)$ and $\Delta d(\gamma, \text{O})$ according to Eq. (6); the results are shown in Figure 4(b). The maximum contrast in a corrugation height profile is obtained for maximum Δd. The maximum contrast between Ru and O atoms is achieved with the maximum difference between $\Delta d(\gamma, \text{Ru}\uparrow)$ and $\Delta d(\gamma, \text{O})$, which is for $\gamma = -10.12\,\text{fNm}^{1/2}$ and $d = 3.65$ Å in Figure 4(b).

In Figure 4(b), we take the Ru↓curve as a reference, which means $\Delta d(\gamma, \text{Ru}\downarrow)$ is always zero. We can plot the corrugation height line profiles Δz based on Figure 4(b). At a given γ and

taking $\Delta d(\gamma,\mathrm{Ru}\downarrow)$ as reference, the Δz for Ru↑ and O can be obtained according to $\Delta d(\gamma,\mathrm{Ru}\uparrow) - \Delta d(\gamma,\mathrm{Ru}\downarrow)$ and $\Delta d(\gamma,\mathrm{O}) - \Delta d(\gamma,\mathrm{Ru}\downarrow)$, respectively. Corrugation height line profiles Δz for three representative values of γ are shown in Figure 5. The maximum corrugation decreases with decreasing γ, from 56.3 pm for $\gamma = -17.6\,\mathrm{fNm}^{1/2}$, 24.6 pm for $\gamma = -10.12\,\mathrm{fNm}^{1/2}$, to 10.9 pm for $\gamma = -1.57\,\mathrm{fNm}^{1/2}$. Although the shape of the corrugation line profiles change somewhat as a function of γ, qualitatively the profile remains the same. The Ru↑ atoms appear as peaks in the profiles, Ru↓ atoms appear as valleys, and the O atoms appear somewhere on the slopes.

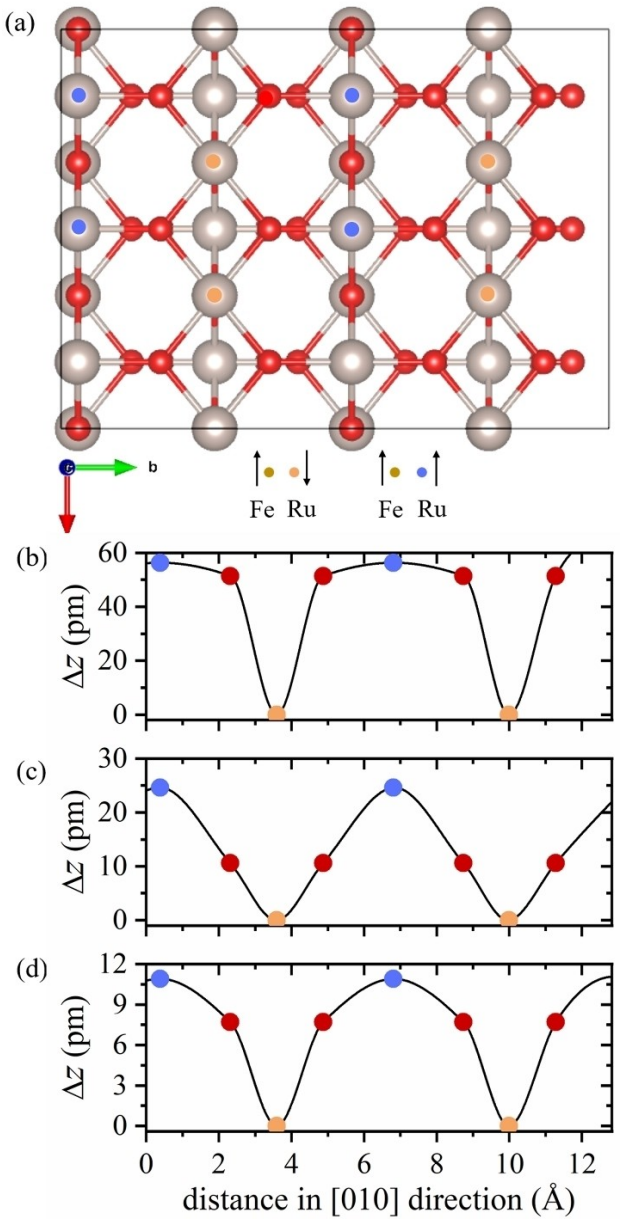

Figure 5. (a) Top view of the RuO_2(110) surface, where orange and blue circles mark the Ru↓ (*p*) and Ru↑ (*ap*) atoms, respectively. Corrugation height line profiles along the [010] (**b**) direction at different frequency shifts (b) $\gamma = -17.6\,\mathrm{fNm}^{1/2}$, (c) $\gamma = -10.12\,\mathrm{fNm}^{1/2}$, and (d) $\gamma = -1.57\,\mathrm{fNm}^{1/2}$. Orange, blue, and red circles correspond to tip positions above Ru↓, Ru↑, and O atoms, respectively. Akima Spline was used to obtain full corrugation profiles.

MExFM experimental measurements on NiO(001) give maximum corrugations of 4.5 pm at $\gamma = -2.55\,\mathrm{fNm}^{1/2}$[13] and 1.1 pm at $\gamma = -0.25\,\mathrm{fNm}^{1/2}$,[17] whereas DFT calculations on the same system give 25 pm at $\gamma = -22.0\,\mathrm{fNm}^{1/2}$.[18,20] These values are comparable to what we find for the RuO_2(110) surface, indicating that the effects are sufficiently large to be measured in MExFM. In contrast to the measurements on NiO(001), however, O atoms will not be visible directly in an MExFM image or corrugation profile. For the RuO_2(110) surface, only the Ru atoms are visible, as they correspond to maxima or minima in the corrugation profile.

Summary

In summary, we have performed DFT calculations to study the exchange interaction between a magnetic Fe tip and an antiferromagnetic RuO_2(110) surface. The exchange forces and energies have been studied as a function of the tip-surface distance. The coupling between tip and surface where the magnetic moments on the Fe tip and the surface Ru atoms are parallel is energetically more favorable than antiparallel coupling. This attractive chemical tip-surface interaction sets in if the tip is sufficiently close to a surface Ru atom, ≲4.5 Å. Upon decreasing the tip-surface distance to ≲2.5 Å, repulsive chemical forces start to dominate. We use the exchange forces to calculate a normalized frequency shift of an oscillating tip positioned over different sites on the surface. These frequency shifts show qualitatively the same trends as a function of tip position and tip-surface distance as the exchange forces.Finally, we construct corrugation height profiles by fixing the frequency shift and extract the points of closest approach of the oscillating tip to a surface atoms for different positions of the tip over the surface. Spin-up Ru atom appear as peaks and spin-down Ru atom appears as valleys in the corrugation height profiles, whereas O atoms will not be directly visible as they do not correspond to maxima or minima. For a reasonable interval of frequency shifts, we obtain corrugation height profiles with amplitudes that are experimentally accessible. From a comparison to the Fe tip-NiO(001) surface case, which has been well-characterized both experimentally and computationally, we predict that the corregation of a RuO_2(110) surface, as observed in a MExFM experiment, should be comparable in size to that of NiO(001).

Supporting Information Description

Figure S1 and Table S1 gives the magnetic moments of the Ru atoms in the RuO_2(110) slab. Figures S2 and S3 present the magnetic moments of the surface the Fe tip and the surface Ru atoms as function of the tip-surface distance. Figure S4 shows the changes in spin density due to the tip-surface interaction, and Figure S5 displays the density of states, projected on the surface Ru atoms, and the tip apex Fe atom. Figure S6 shows

the orbital-resolved density of states, projected on the surface Ru atoms.

Notes

The authors declare no competing financial interest.

Acknowledgements

Q. Liang acknowledges funding from the China Scholarship Council (CSC) (No. 201708450082). This work was carried out on the Dutch national e-infrastructure with the support of SURF Cooperative. Michael Verhage and Dr. Kees Flipse, Technical University Eindhoven, the Netherlands, are thanked for fruitful discussions.

Conflict of Interest

The authors declare no conflict of interest.

Data Availability Statement

The data that support the findings of this study are available from the corresponding author upon reasonable request.

Keywords: density functional calculations · antiferromagnetic RuO_2 · Fe tip · exchange energy and force · corrugation height line profiles

[1] R. R. Rao, M. J. Kolb, N. B. Halck, A. F. Pedersen, A. Mehta, H. You, K. A. Stoerzinger, Z. Feng, H. A. Hansen, H. Zhou, L. Giordano, J. Rossmeisl, T. Vegge, I. Chorkendorff, I. E. L. Stephens, Y. Shao-Horn, *Energy Environ. Sci.* **2017**, *10*, 2626–2637.
[2] D. Teschner, G. Novell-Leruth, R. Farra, A. Knop-Gericke, R. Schlögl, L. Szentmiklósi, M. G. Hevia, H. Soerijanto, R. Schomäcker, J. Pérez-Ramírez, N. López, *Nat. Chem.* **2012**, *4*, 739–745.
[3] S. Kim, G. Evmenenko, Y. Xu, D. B. Buchholz, M. Bedzyk, K. He, J. Wu, V. P. Dravid, *Adv. Funct. Mater.* **2018**, *28*, 1805723.
[4] C.-C. Hu, K.-H. Chang, M.-C. Lin, Y.-T. Wu, *Nano Lett.* **2006**, *6*, 2690–2695.
[5] H. Over, *Chem. Rev.* **2012**, *112*, 3356–3426.
[6] H. Over, Y. D. Kim, A. P. Seitsonen, S. Wendt, E. Lundgren, M. Schmid, P. Varga, A. Morgante, G. Ertl, *Science.* **2000**, *287*, 1474–1476.
[7] C. Xu, Y. Jiang, D. Yi, H. Zhang, S. Peng, J. Liang, *J. Am. Ceram. Soc.* **2014**, *97*, 3702–3709.
[8] W. D. Ryden, A. W. Lawson, *J. Chem. Phys.* **1970**, *52*, 6058–6061.
[9] T. Berlijn, P. C. Snijders, O. Delaire, H. D. Zhou, T. A. Maier, H. B. Cao, S. X. Chi, M. Matsuda, Y. Wang, M. R. Koehler, P. R. C. Kent, H. H. Weitering, *Phys. Rev. Lett.* **2017**, *118*, 077201.
[10] Z. H. Zhu, J. Strempfer, R. R. Rao, C. A. Occhialini, J. Pelliciari, Y. Choi, T. Kawaguchi, H. You, J. F. Mitchell, Y. Shao-Horn, R. Comin, *Phys. Rev. Lett.* **2019**, *122*, 017202.
[11] E. Torun, C. M. Fang, G. A. de Wijs, R. A. de Groot, *J. Phys. Chem. C* **2013**, *117*, 6353–6357.
[12] Q. Liang, G. Brocks, A. Bieberle-Hütter, *J. Phys. Chem. C* **2022**, *126*, 1337–1345.
[13] U. Kaiser, A. Schwarz, R. Wiesendanger, *Nature.* **2007**, *446*, 522–525.
[14] R. Schmidt, C. Lazo, H. Hölscher, U. H. Pi, V. Caciuc, A. Schwarz, R. Wiesendanger, S. Heinze, *Nano Lett.* **2009**, *9*, 200–204.
[15] R. Schmidt, C. Lazo, U. Kaiser, A. Schwarz, S. Heinze, R. Wiesendanger, *Phys. Rev. Lett.* **2011**, *106*, 257202.
[16] R. Schmidt, A. Schwarz, R. Wiesendanger, *Appl. Phys. Lett.* **2017**, *110*, 061601.
[17] F. Pielmeier, F. J. Giessibl, *Phys. Rev. Lett.* **2013**, *110*, 266101.
[18] M. Granovskij, A. Schrön, F. Bechstedt, *Phys. Rev. B* **2013**, *88*, 184416.
[19] H. Momida, T. Oguchi, *Surf. Sci.* **2005**, *590*, 42–50.
[20] M. Granovskij, A. Schrön, F. Bechstedt, *New J. Phys.* **2014**, *16*, 023020.
[21] C. Lazo, S. Heinze, *Phys. Rev. B* **2011**, *84*, 144428.
[22] P. E. Blöchl, *Phys. Rev. B.* **1994**, *50*, 17953–17979.
[23] G. Kresse, D. Joubert, *Phys. Rev. B* **1999**, *59*, 1758–1775.
[24] G. Kresse, J. Furthmüller, *Phys. Rev. B* **1996**, *54*, 11169–11186.
[25] J. P. Perdew, K. Burke, M. Ernzerhof, *Phys. Rev. Lett.* **1996**, *77*, 3865–3868.
[26] S. L. Dudarev, G. A. Botton, S. Y. Savrasov, C. J. Humphreys, A. P. Sutton, *Phys. Rev. B* **1998**, *57*, 1505–1509.
[27] X. Zhang, C. Cao, A. Bieberle-Hütter, *J. Phys. Chem. C* **2016**, *120*, 28694–28700.
[28] L. F. Mattheiss, *Phys. Rev. B.* **1976**, *13*, 2433–2450.
[29] C. Kittel, P. McEuen, P. McEuen, *Introduction to solid state physics*, Wiley New York, **1996**.
[30] C. Lazo, V. Caciuc, H. Hölscher, S. Heinze, *Phys. Rev. B* **2008**, *78*, 214416.
[31] D. Çakır, D. M. Otálvaro, G. Brocks, *Phys. Rev. B* **2014**, *90*, 245404.
[32] E. Vedmedenko, Q. Zhu, U. Kaiser, A. Schwarz, R. Wiesendanger, *Phys. Rev. B* **2012**, *85*, 174410.
[33] N. Hauptmann, S. Haldar, T.-C. Hung, W. Jolie, M. Gutzeit, D. Wegner, S. Heinze, A. A. Khajetoorians, *Nat. Commun.* **2020**, *11*, 1197.
[34] F. J. Giessibl, *Phys. Rev. B.* **1997**, *56*, 16010–16015.
[35] M. Schmid, J. Mannhart, F. J. Giessibl, *Phys. Rev. B* **2008**, *77*, 045402.
[36] F. J. Giessibl, *Rev. Mod. Phys.* **2003**, *75*, 949–983.

Manuscript received: June 21, 2022
Revised manuscript received: October 12, 2022
Accepted manuscript online: November 15, 2022
Version of record online: December 2, 2022

RESEARCH ARTICLE

Corrugation height line profile Δz of the $RuO_2(110)$ surface along the [010] direction is determined using density functional theory calculations.

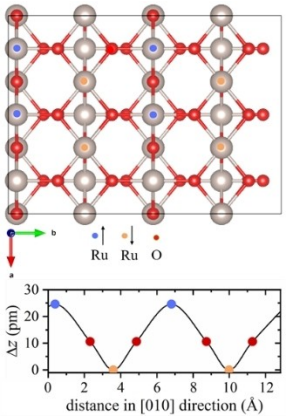

Dr. Q. Liang, Prof. Dr. G. Brocks, Dr. A. Bieberle-Hütter**